RSC Advances

PAPER

View Article Online
View Journal | View Issue

Cite this: *RSC Adv.*, 2017, **7**, 41830

First hyperpolarizabilities of Pt(4-ethynylbenzo-15-crown-5)$_2$(bpy) derivatives with the complexation of mono-cations (Li^+, Na^+, K^+) and di-cations (Mg^{2+}, Ca^{2+}): development of a cation detector†

Hai-Ling Yu, *[a] Wen-Yong Wang,[b] Bo Hong,[a] Yan-Ling Si,[a] Tian-Liang Ma[a] and Ran Zheng[a]

Received 2nd May 2017
Accepted 14th August 2017

DOI: 10.1039/c7ra04919f

rsc.li/rsc-advances

Square-planar platinum(II) compounds containing two crown ethers play an important role in the development of nonlinear optical (NLO) materials, liquid crystals, luminescent materials and also in supramolecular chemistry owing to their diverse charge transfer excited states. The coordination of mono-cationic (Li^+, Na^+, K^+) and di-cationic (Mg^{2+}, Ca^{2+}) metals onto the crown seems to be advantageous for the design of NLO-based cation detectors. Pt(4-ethynylbenzo-15-crown-5)$_2$(bpy) (**L**) and its cation derivatives have been investigated by the density functional theory. The binding of alkali metal cations obviously shrinks the crown ethers due to their strong interaction energies and distorts the crown ethers perpendicular to the bipyridine and Pt plane. Significantly, as compared with **L**, an obvious decrease appears in the first hyperpolarizability after cation complexing. This can be explained by their variable charge transfer transitions along the *y*-axis in conjunction with the distribution of holes and electrons. Thus, it can be noted that square-planar platinum(II) compounds merit the widespread use in the fields of optical detectors.

1. Instruction

Over the past 15 years, there has been increasing interest in the properties of square-planar platinum(II) compounds. One key reason is that square-planar platinum(II) complexes exhibit a variety of charge transfer (CT) excited states[1–9] such as metal-to-ligand charge transfer (MLCT), ligand-to-ligand charge transfer (LLCT), and intraligand charge transfer (ILCT). The directional nature of the CT excited states in square-planar platinum(II) complexes is ideal for hole–electron creation and separation, and consequently, these systems merit the considerable use in numerous fields of materials chemistry, including nonlinear optics (NLO), liquid crystals, conducting polymers, luminescent materials, and supramolecular chemistry.[10–14] There is a library for platinum(II) compounds with various structures, such as mononuclear, dinuclear, and metallacyclic structures, showing their unique physical, optical, photophysical, conductive, as well as self-assembly properties.[15,16] A classical example of the mononuclear square-planar Pt(II) complexes is the platinum(II) alkynyl bipyridine complexes. Because these complexes were found to exhibit a very broad and strong nonlinear absorption in the visible to NIR region, they have potential applications as broadband nonlinear materials.[17]

The photophysical and electrochemical properties of the platinum(II) alkynyl bipyridine complexes are found to be sensitive to the nature of both platinum(II) bipyridine and ancillary ligands. With this regard, the coordination of two 4-ethynylbenzo-15-crown-5 ancillary ligands onto the platinum(II) center[18] seems to be advantageous for the development of NLO-based cation detectors.[19] Because this type of complexes are agreeable with the NLO-based detecting cations devices that must comprise a signaling moiety (platinum atom and bipyridine as the main part that generates NLO signals) and a cation binding site (*e.g.* crown ether moieties, usually termed as the receptor). Since Pedersen first reported the synthesis of crown ethers in 1967,[20] they occupy a special position in the development of receptors and are widely used in the design of new optical detectors[21–23] based on their unique ability to coordinate the cations of alkali and alkaline metals (such as Li^+, Na^+, K^+, Mg^{2+} and Ca^{2+}),[24–27] along with their fairly high selectivity and accessibility.[28]

Despite the fact that considerable works on the development of platinum(II) complexes as NLO materials have been reported,[29–32] works on the design of NLO-based detecting complexes with alkali cations have received less attention. An efficient NLO-based detector should exhibit a substantial

[a]*College of Resources and Environmental Science, Jilin Agricultural University, Changchun 130118, People's Republic of China. E-mail: jlauyu@163.com*

[b]*JiangSu XinHai Senior High School, Lianyungang City 222000, Jiangsu, People's Republic of China*

† Electronic supplementary information (ESI) available. See DOI: 10.1039/c7ra04919f

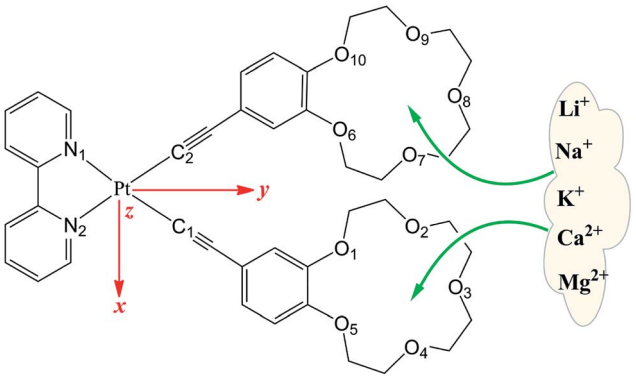

Fig. 1 Structures of [Pt(4-ethynylbenzo-15-crown-5)$_2$(bpy)] (bpy = 2,2′-bipyridine) (**L**) and its metal cation derivatives.

"switch-on" or "switch-off" effect upon binding to metal ions. The platinum(II) alkynyl bipyridine complexes and its metal cation derivatives have displayed an obvious contrast in NLO properties. As part of our continuing interest in the design of new NLO-based detectors with crown ether and its corresponding alkali cation derivatives,[33] [Pt(4-ethynylbenzo-15-crown-5)$_2$(bpy)] (bpy = 2,2′-bipyridine) (**L**) was chosen as a parent compound. The platinum(II) alkynyl bipyridine complexes along with its mono-cations (Li^+, Na^+, and K^+) and di-cations alkaline metal (Mg^{2+} and Ca^{2+}) derivatives (Fig. 1) were investigated using the density functional theory (DFT) with the aim of rationalizing their geometrical and nonlinear optical properties. It is expected that the complexation of **L** with alkali metals will trigger the modulation of NLO properties such as the first hyperpolarizability. In this case, cation detection is possible by monitoring NLO intensity, which may be of interest for the development of NLO-based probes.

2. Computation details

DFT calculations were performed using the Gaussian 09W program.[34] The geometry optimizations of all molecules were fully optimized at the B3LYP functional with the 6-31G** basis set for C, H, and O atoms, 6-311G** for Li, Na, K, Mg, and Ca atoms and the LanL2DZ effective core potential (ECP) basis set for Pt atom. The B3LYP function was used because it successfully reproduced the experimental structures.[35,36] All optimized structures reached the true local minimum stationary points. Because there is no imaginary frequency. Interaction energies, enthalpy, Gibbs free energies and natural population analysis (NPA) charge are calculated at the B3LYP/6-31G**/LanL2DZ level.

Due to the efficiency and accuracy, the first hyperpolarizability β is calculated by analytical third energy derivatives. The total first hyperpolarizability (β_{tot}) is defined as

$$\beta_{tot} = \sqrt{\left(\beta_x^2 + \beta_y^2 + \beta_z^2\right)} \quad (1)$$

where β_i is defined as

$$\beta_i = (1/3)\sum_j \left(\beta_{ijj} + \beta_{jji} + \beta_{jij}\right) \quad i, j = \{x,\ y,\ z\} \quad (2)$$

DFT calculations, using conventional functions, sometimes fail to correctly predict the amplitude of hyperpolarizability, which is the result of their wrong asymptotic exchange potentials.[37,38] The long-range correct LC-BLYP and CAM-B3LYP functionals are good options for the calculation of hyperpolarizabilities.[39] For a contrastive study, the hyperpolarizabilities were also evaluated by the M06-2X functional.[40] The basis set used is 6-311+G** except LanL2DZ ECP basis set for Pt atom.

The hyper-Rayleigh scattering (HRS) response is one of the second-order NLO phenomena. Champagne and co-workers[41–48] developed an effective method to evaluate the HRS response $\beta_{HRS}(-2\omega;\omega,\omega)$, which is described as

$$\beta_{HRS}(-2\omega;\omega,\omega) = \sqrt{\langle\beta_{ZZZ}^2\rangle + \langle\beta_{ZXX}^2\rangle} \quad (3)$$

where $\langle\beta_{ZZZ}^2\rangle$ and $\langle\beta_{ZXX}^2\rangle$ are the orientational average of the molecular β tensor components, which can be calculated using the following equations:

$$\langle\beta_{ZZZ}^2\rangle = \frac{1}{7}\sum_{\zeta}^{x,y,z}\beta_{\zeta\zeta\zeta}^2 + \frac{6}{35}\sum_{\zeta\neq\eta}^{x,y,x}\beta_{\zeta\zeta\zeta}\beta_{\zeta\eta\eta} + \frac{9}{35}\sum_{\zeta\neq\eta}^{x,y,z}\beta_{\eta\zeta\zeta}^2 + \frac{3}{35}\sum_{\zeta\neq\eta\neq\xi}^{x,y,x}\beta_{\eta\zeta\zeta}\beta_{\eta\xi\xi} + \frac{2}{35}\sum_{\zeta\neq\eta\neq\xi}^{x,y,z}\beta_{\zeta\eta\xi}^2 \quad (4)$$

$$\langle\beta_{ZXX}^2\rangle = \frac{1}{35}\sum_{\zeta}^{x,y,z}\beta_{\zeta\zeta\zeta}^2 - \frac{2}{105}\sum_{\zeta\neq\eta}^{x,y,x}\beta_{\zeta\zeta\zeta}\beta_{\zeta\eta\eta} + \frac{11}{105}\sum_{\zeta\neq\eta}^{x,y,z}\beta_{\eta\zeta\zeta}^2 - \frac{1}{105}\sum_{\zeta\neq\eta\neq\xi}^{x,y,x}\beta_{\eta\zeta\zeta}\beta_{\eta\xi\xi} + \frac{4}{105}\sum_{\zeta\neq\eta\neq\xi}^{x,y,z}\beta_{\zeta\eta\xi}^2 \quad (5)$$

In addition, the depolarization ratio (DR), which gives the molecular geometric information, is responsible for the NLO response and expressed as

$$DR = \frac{\langle\beta_{ZZZ}^2\rangle}{\langle\beta_{ZXX}^2\rangle} \quad (6)$$

The first hyperpolarizability can also be obtained using the sum-over-states (SOS) methods.[49] SOS method is used to separate and discuss the contribution from different excited states. The first hyperpolarizability β of SOS equation can be expressed as follows:[50]

$$\beta_{ABC}(-\omega_\sigma;\omega_1,\omega_2) = \hat{P}\left[A(-\omega_\sigma),B(\omega_1),C(\omega_2)\right]\sum_{i\neq 0}\times\sum_{j\neq 0}\frac{\mu_{0i}^A\overline{\mu_{ij}^B}\mu_{j0}^C}{(\Delta_i-\omega_\sigma)(\Delta_j-\omega_2)} \quad (7)$$

$$\mu_{ij}^A = \left\langle i\left|\hat{\mu}^A\right|j\right\rangle\overline{\mu_{ij}^A} = \mu_{ij}^A - \mu_{00}^A\delta_{ij}\omega_\sigma = \sum_i\omega_i \quad (8)$$

where A, B, and C denote one of directions of x, y and z, ω is energy of external fields ($\omega = 0$ corresponds to static electric field), Δ_i is defined as excitation energy of state i with respect to ground state (0). $\hat{P}$ is permutation operator (for β, there are 3! = 6 permutations). μ_{ij}^A represents the A component of transition dipole moment between state i and j (when $i = j$, the term

simply corresponds to electric dipole moment of state i), and $\hat{\mu}$ is dipole moment operator (*e.g.*, $\hat{\mu}^x \equiv -x$).

The properties of the excited states were investigated by employing the time-dependent density functional theory (TDDFT), which incorporates electronic screening and relevant correction effect for electronic excitation, to evaluate the excited states.[51,52] All electronic excited states are calculated at the CAM-B3LYP/6-311+G**/LanL2DZ level since CAM-B3LYP functional is in satisfactory agreement with the experimental values.[53]

The NPA charge is evaluated from natural bond orbital (NBO) population analysis using NBO program embedded in Gaussian 09W program, while the charge density difference (CDD) on a surface around a molecule is calculated by the Multiwfn 3.3.8 software.[54]

3. Results and discussion

3.1 Geometrical structure and thermodynamic analysis

The structures of **L**, **L***$(Li^+)_2$, **L***$(Na^+)_2$, **L***$(K^+)_2$, **L***$(Ca^{2+})_2$ and **L***$(Mg^{2+})_2$ were optimized at the B3LYP/6-31G** level. The minimum vibrational frequencies of these structures are 1.54, 5.8, 5.48, 3.14, 6.07 and 6.39 cm^{-1}. The small vibration amplitude supports the fact that the optimized structures are thermally stable and at minimum. Selected bond lengths of Pt–C and Pt–N bonds and average O–O bond lengths of crown ethers are listed in Table 1. The Pt–C and Pt–N bond deviations between **L** and its corresponding experimental values are 0.029 Å and 0.058 Å, respectively, whereas O–O bond deviation is in the range from 0.018 Å to 0.019 Å. As seen from the result, the geometrical parameters of **L** are very close to the experimental values previously reported by Chi-Ming Che determined from the crystallographic study,[55] suggesting that the geometrical calculation of B3LYP method is reliable. For Pt–C and Pt–N bonds, the bond lengths of **L** are 1.952 Å and 2.120 Å, respectively. In contrast, the Pt–C and Pt–N bonds in metal cation derivatives are slightly longer, reflecting the minimal impact of metal cations on Pt–C and Pt–N bonds. However, as compared with those in **L**, the average O–O bond lengths of metal cation derivatives became smaller. The deviation of O–O bond lengths between metal cation derivatives and **L** is in the order of **L***$(Li^+)_2$ > **L***$(Na^+)_2$ > **L***$(K^+)_2$ and **L***$(Mg^{2+})_2$ > **L***$(Ca^{2+})_2$. This indicates that the crown ethers shrink obliviously, especially in **L***$(Li^+)_2$ and **L***$(Mg^{2+})_2$. This is easy to understand since metal cations have strong interactions with crown ethers. The metal cations also distort the crown ether moieties perpendicular to the bipyridine and Pt plane, which is clearly seen from Fig. S1 in the ESI.†

Table 2 Enthalpy and Gibbs free energies of complexation reaction (kcal mol^{-1} at 298.15 K and 1 atm) calculated at the B3LYP/6-31G**/LanL2DZ level

Complex	ΔH^0	ΔG^0
L*$(Li^+)_2$	−207.5	−198.3
L*$(Na^+)_2$	−156.9	−142.0
L*$(K^+)_2$	−94.6	−80.9
L*$(Mg^{2+})_2$	−616.2	−604.3
L*$(Ca^{2+})_2$	−428.7	−413.3

Interaction energies between **L** and metal cations were considered at the B3LYP/6-31G** level. The results in Table 1 reveal that all complexes have large and negative values of interaction energies, indicating the stability of alkali metal cations derivatives and strong interactions between metal cations and crown ethers. For mono-cation derivatives, the interaction energies are −120.2 kcal mol^{-1} (**L***$(Li^+)_2$) < −92.9 kcal mol^{-1} (**L***$(Na^+)_2$) < −63.3 kcal mol^{-1} (**L***$(K^+)_2$), which are two times higher compared to the values reported by Gao.[56] This is reasonable since **L** and its metal cation derivatives have two crown ether fragments, and the interaction energy is the sum of two interaction energies between the crown ether and metal cation.

The interaction energies present the same sequence of the deviation of O–O bond lengths. The smaller interaction energy of complex **L***$(K^+)_2$ can be attributed to its structure of K atoms out of the plane of the five O atoms of the crown ethers. Moreover, for di-cations derivatives, the interaction energies are −326.7 kcal mol^{-1} (**L***$(Mg^{2+})_2$) < −230.6 kcal mol^{-1} (**L***$(Ca^{2+})_2$), which holds the same truth with the deviation of O–O bond lengths. These values support the oblivious influence of alkali metal cations and the degree of the shrinkage on the crown ethers.

Table 2 summarizes the main thermodynamic data for the complexation reaction of the alkali ion by the **L** form. The Gibbs

Table 1 Important geometrical parameters and interaction energies (kcal mol^{-1}) calculated at the B3LYP/6-31G**/LanL2DZ level (bond length and dihedral angle are in Å and °, respectively)

Compound	Pt–C1	Pt–C2	Pt–N1	Pt–N2	O–O (1)[a]	O–O (2)[b]	E_{int}
L	1.952 (1.981)[c]	1.952 (1.981)[c]	2.120 (2.062)[c]	2.120 (2.062)[c]	2.843 (2.861)[c]	2.842 (2.861)[c]	—
L*$(Li^+)_2$	1.954	1.954	2.125	2.125	2.599	2.599	−120.2
L*$(Na^+)_2$	1.954	1.954	2.124	2.124	2.727	2.728	−92.9
L*$(K^+)_2$	1.954	1.954	2.125	2.125	2.767	2.768	−63.3
L*$(Mg^{2+})_2$	1.957	1.957	2.128	2.128	2.516	2.516	−326.7
L*$(Ca^{2+})_2$	1.957	1.957	2.128	2.128	2.706	2.706	−230.6

[a] Average O–O bond length of the O_1–O_2, O_2–O_3, O_3–O_4, O_4–O_5 and O_5–O_1 bonds. [b] Average O–O bond length of the O_6–O_7, O_7–O_8, O_8–O_9, O_9–O_{10} and O_{10}–O_{11} bonds. [c] Values in the bracket are determined by X-ray analysis from ref. 55.

free energies ($T = 298.15$ K and $P = 1$ atm) of these reaction are exothermic, and the most exothermic reaction is the complexation of the Mg^{2+} and Ca^{2+} cations. Note that the Gibbs free energies (in absolute value) decrease monotonically with the cation size for mono-cations (Li^+, Na^+, K^+) and di-cations (Mg^{2+}, Ca^{2+}) complexes, which is similar with the trend of interaction energy. Indeed, the enthalpy also behaves similarly as the cation size.

3.2 Charge distribution

Atomic charge is one of the simplest and most intuitive description of charge distribution and has great significance in theory and practical applications.[57] The global charge of the different fragments (F*i*) of compounds **L** and its metal cation derivatives was computed at the B3LYP/6-31G**/LanL2DZ level using the NPA method (Table S1, ESI†). For all compounds, the negative charge is mainly located at the crown ether (F1, F2) and alkynyl (F5, F6) moieties, which is respectively attributed to the large electronegativity of oxygen and the rich electron-density of π conjunction. The negative charge and cavity of crown ether of **L** lead to its ability to coordinate the cations of alkali metals. In contrast, the benzene (F3, F4), bipyridine (F8) and Pt (F7) moieties are positively charged. Upon complexing with alkali metal cation, all fragments (F1 to F8) become positive and the electron density decreases (Fig. 2) because the complexation leads mainly to electron transfer from all fragments to an alkali metal cation. The most modification of the charge distribution is the crown ether (F1, F2), benzene (F3, F4), and bipyridine (F8) moieties. For the crown ether (F1, F2) moieties, the modification decreases monotonically with the cation size of mono-cations (Li^+, Na^+, K^+) and di-cations (Mg^{2+}, Ca^{2+}), respectively. In cases of Pt (F7) atoms and alkynyl (F5, F6) moieties, they play the role of spectator and are almost unaffected by the complexation. Thus, the coordination of alkali metal cation onto **L** is also characterized by charge reorganizations.

3.3 First hyperpolarizability

At the molecular level, the second-order NLO response comes from the second-order NLO coefficient, *i.e.* the first hyperpolarizability (β). Previous theoretical investigations have revealed that the second-order NLO properties of crown ether

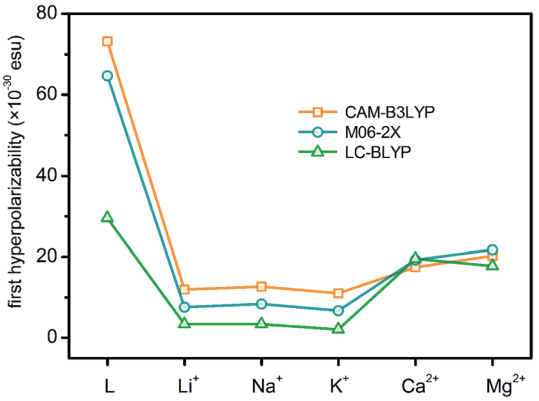

Fig. 3 First hyperpolarizability of L and its cation derivatives.

derivatives can be switched by cation complexing.[33] By combining the switches of nonlinear optical responses, macrocyclic crown ethers present a more practical and reliable chance to be a cation detector. In order to rationalize the different NLO behaviors of **L** and its metal cation derivatives, the first hyperpolarizabilities of six molecules have been calculated theoretically at the DFT/6-311++G** levels using the CAM-B3LYP, M06-2X and LC-BLYP functionals. The results are reported in Fig. 3 and Tables S2–S5 (ESI).† Comparison to CAM-B3LYP functional, the M06-2X and LC-BLYP functionals seem to underestimate the first hyperpolarizabilities with the exception of $\mathbf{L^*(Mg^{2+})_2}$ and $\mathbf{L^*(Ca^{2+})_2}$ ($\mathbf{L^*(Mg^{2+})_2} \approx \mathbf{L^*(Ca^{2+})_2}$). However, the first hyperpolarizabilities obtained with three functionals show the similar decrease trends of $\mathbf{L} > \mathbf{L^*(Mg^{2+})_2} \approx \mathbf{L^*(Ca^{2+})_2} > \mathbf{L^*(Li^+)_2} \approx \mathbf{L^*(Na^+)_2} > \mathbf{L^*(K^+)_2}$, demonstrating the relative reliability of three DFT methods. Therefore, in the next discussion, only the CAM-B3LYP functional is taken as an example to shed light on the change of the first hyperpolarizability. All first hyperpolarizabilities are calculated with the ultrafine integration grid (99, 590). The first hyperpolarizabilities are also calculated at the CAM-B3LYP level with the superfine grid (the superfine grid specification is (150, 974) for the first two rows of the periodic table and (225, 974) for later elements) (Table S3, ESI†) to check the convergence of the size of the integration grid. The first hyperpolarizabilities of the ultrafine grid are almost consistent with the values of the superfine

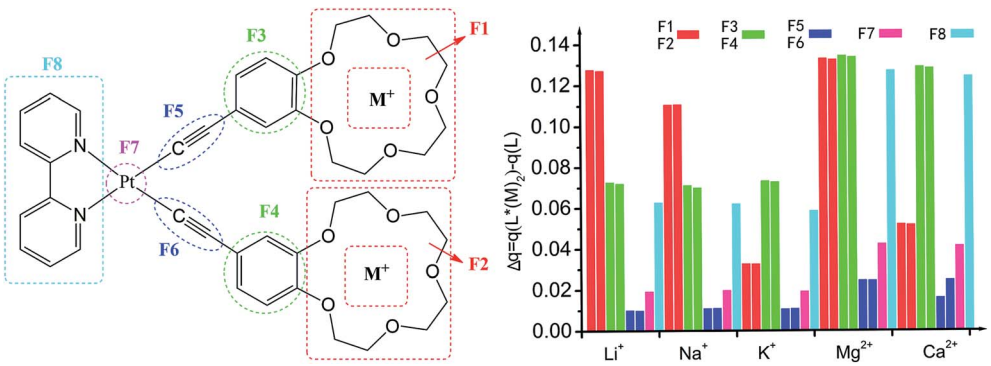

Fig. 2 The NPA charge for the fragments (S1–S8) of L and $L^*(M^{+/2+})_2$ determined at the B3LYP/6-31G*/LanL2DZ level, $\Delta q = q(L^*(M^{+/2+})_2) - q(L)$.

Table 3 Static ($\lambda = \infty$) and dynamic ($\lambda = 1064$ nm) HRS first hyperpolarizabilities (10^{-30} esu), depolarization ratios as well as their β_{HRS}(L)/β_{HRS}(L*(M$^{+/2+}$)$_2$) contrast ratios calculated at the CAM-B3LYP/6-311+G**/LanL2DZ levels

	∞		1064		∞
	β_{HRS}	DR	β_{HRS}	DR	β_{HRS}(L)/β_{HRS}(L*(M$^{+/2+}$)$_2$)
L	28.0	6.8	124.3	8.7	—
L*(Li$^+$)$_2$	6.4	2.8	14.1	3.8	4.4
L*(Na$^+$)$_2$	6.6	3.0	15.1	4.1	4.2
L*(K$^+$)$_2$	6.3	2.6	15.0	4.0	4.4
L*(Mg^{2+})$_2$	11.6	2.2	18.6	2.1	2.4
L*(Ca^{2+})$_2$	13.0	2.3	20.9	2.2	2.2

grid, indicating that the ultrafine integration grid is acceptable and convergent.

First hyperpolarizability is a third rank tensor that can be described by a 3 × 3 × 3 matrix. For the static first hyperpolarizability, the 3 × 3 × 3 = 27 components can be reduced to 10 components by Kleinman's symmetry. With these 10 components, the contribution of each one to the first hyperpolarizability is obtained. The β values in three Cartesian axes, which directly reflect the direction of the charge transfer, can also be calculated. The important components of the first hyperpolarizability are listed as ESI (Tables S2–S5).† As seen from the results, the β_{xxy} and β_{yyy} tensorial components with some contribution of β_{yyz} are the dominant ones that describe the β_{tot} values with respect to the rest tensorial components, which inevitably leads to the largest β_y tensorial component. For **L**, **L*(Li$^+$)$_2$**, **L*(Na$^+$)$_2$** and **L*(K$^+$)$_2$**, the β_y values are positive, whereas for **L*(Mg^{2+})$_2$** and **L*(Ca^{2+})$_2$**, the β_y values are negative. It suggests that during a polarization process, the direction of electronic charge transition among **L**, **L*(Li$^+$)$_2$**, **L*(Na$^+$)$_2$**, **L*(K$^+$)$_2$** and **L*(Mg^{2+})$_2$**, **L*(Ca^{2+})$_2$** is opposite. It is expected that the electronic charge transition is migrated from 2,2′-bipyridine and Pt moieties (15-crown-5 moiety) to the 15-crown-5 moiety (2,2′-bipyridine moiety) since the β_y values are positive (negative). For the metal cation derivatives, the first hyperpolarizabilities shown in Fig. 3 are insensitive to the alkali metals in the same group. However, an obviously decrease in β after cation complexing is observed with respect to compound **L**. It reveals that the first hyperpolarizability is sensitive to the cation complexing.

Table 3 reports the static and dynamic ($\lambda = 1064$ nm) HRS first hyperpolarizabilities (β_{HRS}) and the depolarization ratios and the β_{HRS} contrast ratios for **L** and its cation derivatives. The variations of the static and dynamic β_{HRS} values are similar to those of β_{tot} values. It can be stated that the cation complexing leads to the small static and dynamic β_{HRS} values, in particular the mono-cations (Li^+, Na^+, K^+) with β_{HRS}(L)/β_{HRS}(L*(M$^{+/2+}$)$_2$) contrast ratio decreases by about a factor of 4.4. It is interesting to note that the effects of alkali/complexation on the β_{HRS} values are much smaller and mainly in different direction of Champagne's investigations.[19,58] In any case, the obvious variations of the first hyperpolarizability contrasts gives complex **L** a chance to access NLO-based detection of cations. When considering the complexation process, the alkali metal cation induces a remarkable decrease in the values of static DR. In the case of di-cations (Mg^{2+}, Ca^{2+}) derivatives, the DR values are even smaller, demonstrating that they depart more from ideal one-dimensional structures of which DR = 5. These variations of DR can be rationalized in terms of a large change of geometrical and electronic structure. Since the measurements are performed at 1064 nm, the dynamic β_{HRS} and DR are calculated at $\lambda = 1064$ nm. As compared with the static β_{HRS} and DR, a strong enhancement is clearly seen at $\lambda = 1064$ nm, in particular in the case of compound **L**. Compound **L** is impacted by electronic resonance since it presents a maximum absorption at 482 and 436 nm, whereas the 532 nm second-harmonic generation wavelength is within the absorption band.

3.4 Analysis of excited state

The SOS method is generally not recommended for evaluation of first hyperpolarizability due to its less accuracy.[59] However, the advantage of SOS is that the contribution from different states can be separated. The combination of the SOS approach (Fig. S2, ESI†) with the low-lying excited states, which contributes obviously to first hyperpolarizability, has been listed in Table 4.

For compound **L**, the S2 excited state has a large contribution to first hyperpolarizability. It is mainly made up of HOMO−1 →

Table 4 Main excited states, transition energies (ΔE, eV), oscillator strengths (f_{os}), and major molecular orbital contributions calculated at the CAM-B3LYP/6-31+G* level

Complex	S	ΔE	f_{os}	MO transition
L	2	2.8436	0.1760	HOMO−1 → LUMO (83%), HOMO−3 → LUMO (10%)
L*(Li$^+$)$_2$	7	4.4291	0.8069	HOMO → LUMO+10 (34%), HOMO−1 → LUMO+9 (15%), HOMO → LUMO+6 (12%)
L*(Na$^+$)$_2$	7	4.4184	0.7504	HOMO → LUMO+10 (18%), HOMO → LUMO+5 (13%), HOMO−1 → LUMO+9 (10%), HOMO → LUMO+8 (10%)
L*(K$^+$)$_2$	7	4.4173	0.7712	HOMO → LUMO+9 (24%), HOMO → LUMO+10 (23%)
L*(Mg^{2+})$_2$	9	4.2446	0.6993	HOMO → LUMO+6 (44%), HOMO−3 → LUMO+5 (22%), HOMO−2 → LUMO+6 (10%)
L*(Ca^{2+})$_2$	9	4.2199	0.7716	HOMO → LUMO+6 (23%), HOMO → LUMO+8 (13%), HOMO−3 → LUMO+5 (12%), HOMO → LUMO+4 (11%)

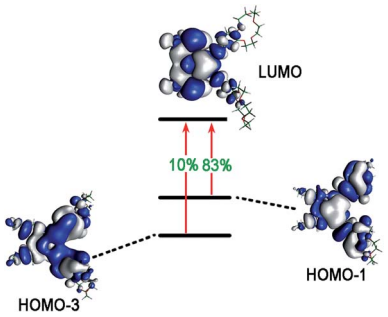

Fig. 4 The molecular orbitals of L involved in the crucial excited states.

LUMO. These molecular orbitals (MO) involved in the main charge transfer transition are illustrated in Fig. 4. It is obvious that the transition of **L** can be assigned to the charge transfer from ethynylbenzo crown moiety to Pt and 2,2′-bipyridine moiety. The direction of charge transfer is opposite to the *y*-axis, which inevitably reflects the positive β_y values. However, for metal cation derivatives, the transition of molecular orbital (MO) pairs is multiple and more complex. The most straightforward way to deal with this problem is to introduce the charge density difference (CDD) between the excited state and ground state (Fig. 5), which can be exactly evaluated as $\Delta\rho(r) = \rho^{ele}(r) - \rho^{hole}(r)$. In single-electron excitation process, an electron leaves A and goes to B, they are named as "hole" and "electron", respectively. The density distribution of holes and electrons are

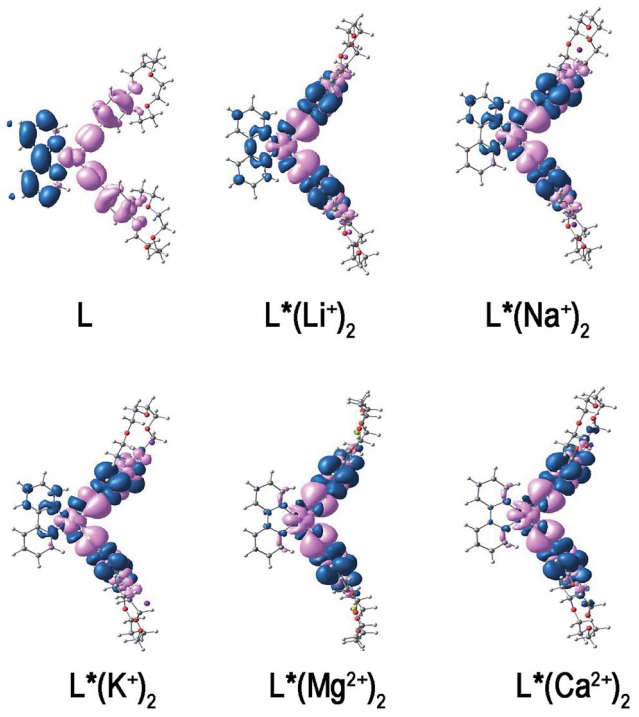

Fig. 5 The CDD between the excited and ground states. Pink and blue colors indicate the depletion and the accumulation of electron density, respectively.

$$\rho^{hole}(r) = \rho^{hole}_{(loc)}(r) + \rho^{hole}_{(cross)}(r) = \sum_{i\to l}\left(w_i^l\right)^2\varphi_i(r)\varphi_i(r) + \sum_{i\to l}\sum_{j\neq i\to l} w_i^l w_j^l \varphi_i(r)\varphi_j(r) \quad (9)$$

$$\rho^{ele}(r) = \rho^{ele}_{(loc)}(r) + \rho^{ele}_{(cross)}(r) = \sum_{i\to l}\left(w_i^l\right)^2\varphi_l(r)\varphi_l(r) + \sum_{i\to l}\sum_{i\to m\neq l} w_i^l w_i^m \varphi_l(r)\varphi_m(r) \quad (10)$$

where "loc" and "cross" stand for the contribution of the local and cross terms to the hole/electron distribution, i and l, respectively, run over all occupied and virtual MOs, w is a configuration coefficient, and φ denotes MO.

From the CDD plots, it is quite obvious that for compound **L**, there is a charge transfer from ethynylbenzo crown moiety to Pt and 2,2′-bipyridine moiety. This result is in accordance with the MO analysis. It suggests that the regions of the density depletion and increment and the electronic transition involved in excited states can be easily identified according to the CDD analysis. For mono-cation (Li^+, Na^+, K^+) derivatives, the distribution of holes is located on the Pt atom and ethynyl moiety, whereas the distribution of electrons is located on the bipyridine moiety with some on the phenyl moiety. Due to the extra and opposite charge transfer from Pt atom and ethynyl moiety to phenyl moiety, the strength of charge transfer to bipyridine moiety is weakened. It then reflects the smaller positive β_y values of mono-cation (Li^+, Na^+, K^+) derivatives. In contrast, the distribution of electrons of di-cations (Mg^{2+}, Ca^{2+}) derivatives is located on the phenyl moiety, while the distribution of holes is located on the Pt atom and ethynyl moiety. Obviously, there is a little confusion between the distribution of holes and electrons. A contrary direction of the charge transfer of di-cations (Mg^{2+}, Ca^{2+}) derivatives is shown as compared to **L** and its mono-cation (Li^+, Na^+, K^+) derivatives. Thus, the β_y values of di-cations (Mg^{2+}, Ca^{2+}) derivatives become smaller and negative.

From the complex SOS expression, Oudar has established the two-level model that linked between β and a low-lying charge transfer transition.[60,61] In this two-level model, the first hyperpolarizability is proportional to the optical intensity and inversely proportional to the cube of the transition energy. Hence, the low excitation energy is the decisive factor in the β value. The transition energies at the low-lying and crucial states, which are contributed the most to the hyperpolarizability, are listed in Table 4. The transition energy increases in the order of **L** < **L*(Mg^{2+})$_2$** ≈ **L*(Ca^{2+})$_2$** < **L*(Li$^+$)$_2$** ≈ **L*(Na$^+$)$_2$** ≈ **L*(K$^+$)$_2$**. As seen from the results, when the metal cation coordinates to **L**, it brings larger transition energy and reduces the possibility of electron transition, thus generates a smaller β value.

4. Conclusion

Systematic DFT calculations have been conducted Pt(4-ethynylbenzo-15-crown-5)$_2$(bpy) (bpy = 2,2′-bipyridine) complex and its derivatives with the complexation of mono-cations (Li^+, Na^+, K^+) and di-cations (Mg^{2+}, Ca^{2+}). The binding of alkali/alkaline metal cations shrinks the crown ether obviously and distort

them perpendicular to the bipyridine and Pt plane. Clearer charge reorganizations are characterized by the coordination of alkali metal cation onto **L**. The complexation of mono-cations and di-cations can induce a significant decrease of the first hyperpolarizability. This first hyperpolarizability contrast can be explained by different charge transfer transition from the standpoint of the distribution of holes and electrons. Therefore, the second-order NLO behaviors can be switched by different groups of alkali metal cations. These results will broaden the scope of the optical molecular detectors and inspired us to investigate further.

Conflicts of interest

There are no conflicts to declare.

Acknowledgements

The authors gratefully acknowledge the financial support from the Science and Technology Research Project of the "13th Five-Year" Education Department of Jilin Province ([2016] 171), the financial support from the National Natural Science Foundation of China (No. 31502109), and the National Natural Science Foundation of China (No. 21503091). Additionally, we gratefully acknowledge the technical support from the group of Professor Yong-Qing Qiu and the usage of the computer and software from the Institute of Functional Material Chemistry of Northeast Normal University.

References

1 V. M. Miskowski and V. H. Houlding, *Inorg. Chem.*, 1991, **30**, 4446–4452.
2 V. M. Miskowski and V. H. Houlding, *Inorg. Chem.*, 1989, **28**, 1529–1533.
3 J. V. Slageren, A. Klein and S. Záliš, *Coord. Chem. Rev.*, 2002, **230**, 193–211.
4 H. Y. Wang, C. Zheng and P. Q. Dai, *RSC Adv.*, 2016, **6**, 114078–114085.
5 A. Klein, J. V. Slageren and S. Záliš, *Eur. J. Inorg. Chem.*, 2003, **10**, 1917–1938.
6 S. W. Lai, M. C. W. Chan, K. K. Cheung and C. M. Che, *Organometallics*, 1999, **18**, 3327–3336.
7 F. Q. Guo, W. F. Sun, Y. Liu and K. Schanze, *Inorg. Chem.*, 2005, **44**, 4055–4065.
8 D. K. Crites Tears and D. R. McMillin, *Coord. Chem. Rev.*, 2001, **211**, 195–205.
9 R. Büchner, J. S. Field and R. J. Haines, *Inorg. Chem.*, 1997, **36**, 3952–3956.
10 J. Manna, C. J. Kuehl, J. A. Whiteford, P. J. Stang, D. C. Muddiman, S. A. Hofstadler and R. D. Smith, *J. Am. Chem. Soc.*, 1997, **119**, 11611–11619.
11 V. W. W. Yam, K. K. W. Lo and K. M. C. Wong, *J. Organomet. Chem.*, 1999, **578**, 3–30.
12 K. Onitsuka, M. Fujimoto, N. Ohshiro and S. Takahashi, *Angew. Chem., Int. Ed.*, 1999, **38**, 689–692.
13 P. Nguyen, P. Gómez-Elipe and I. Manners, *Chem. Rev.*, 1999, **99**, 1515–1548.
14 U. Belluco, R. Bertani, R. A. Michelin and M. Mozzon, *J. Organomet. Chem.*, 2000, **600**, 37–55.
15 K. M. C. Wong and V. W. W. Yam, *Acc. Chem. Res.*, 2011, **44**, 424–434.
16 V. W. W. Yam and K. M. C. Wong, *Chem. Commun.*, 2011, **47**, 11579–11592.
17 V. W. W. Yam, V. K. M. Au and S. Y. L. Leung, *Chem. Rev.*, 2015, **115**, 7589–7728.
18 P. K. M. Siu, S. W. Lai, W. Lu, N. Y. Zhu and C. M. Che, *Eur. J. Inorg. Chem.*, 2003, **3**, 2749–2752.
19 B. Champagne, A. Plaquet, J. L. Pozzo, V. Rodriguez and F. Castet, *J. Am. Chem. Soc.*, 2012, **134**, 8101–8103.
20 C. J. Pedersen, *J. Am. Chem. Soc.*, 1967, **89**, 2495–2496.
21 H. G. Löhr and F. Vögtle, *Acc. Chem. Res.*, 1985, **18**, 65–72.
22 A. P. de Silva, H. Q. N. Gunaratne, T. Gunnlaugsson, A. J. M. Huxley, C. P. McCoy, J. T. Rice and T. E. Rice, *Chem. Rev.*, 1997, **97**, 1515–1566.
23 B. Valeur and I. Leray, *Coord. Chem. Rev.*, 2000, **205**, 3–40.
24 R. Boulatov, B. Du, E. A. Meyers and S. G. Shore, *Inorg. Chem.*, 1999, **38**, 4554–4558.
25 S. T. Liddle and K. Izod, *Organometallics*, 2004, **23**, 5550–5559.
26 Y. Lp, J. Yamauchi and N. Azuma, *J. Coord. Chem.*, 1997, **42**, 291–301.
27 C. Lichtenberg, P. Jochmann, T. P. Spaniol and J. Okuda, *Angew. Chem., Int. Ed.*, 2011, **50**, 5753–5756.
28 C. I. C. Esteves, R. M. F. Batista, M. M. M. Raposo and S. P. G. Costa, *Dyes Pigm.*, 2016, **135**, 134–142.
29 M. Y. Zhang, C. H. Wang, W. Y. Wang, N. N. Ma, S. L. Sun and Y. Q. Qiu, *J. Phys. Chem. A*, 2013, **117**, 12497–12510.
30 A. A. Melekhova, D. V. Krupenya, V. V. Gurzhiy, A. S. Melnikov, P. Y. Serdobintsev, S. I. Selivanov and S. P. Tunik, *J. Organomet. Chem.*, 2014, **763–764**, 1–5.
31 Y. Fan and D. Zhao, *ACS Appl. Mater. Interfaces*, 2015, **7**, 6162–6171.
32 C. Makedonas and C. A. Mitsopoulou, *Inorg. Chim. Acta*, 2007, **360**, 3997–4009.
33 H. L. Yu, W. Y. Wang, B. Hong, Y. Zong and Y. L. Si, *Phys. Chem. Chem. Phys.*, 2016, **18**, 26487–26494.
34 M. J. Frisch, G. W. Trucks, H. B. Schlegel, G. E. Scuseria, M. A. Robb, J. R. Cheeseman, G. Scalmani, V. Barone, B. Mennucci and G. A. Petersson, *Gaussian 09, Revision D.01*, Gaussian, Inc., Wallingford, CT, 2009.
35 D. Herebian, K. E. Wieghardt and F. Neese, *J. Am. Chem. Soc.*, 2003, **125**, 10997–11005.
36 D. Espa, L. Pilia, L. Marchiò, F. Artizzu, A. Serpe, M. L. Mercuri, D. Simão, M. Almeida, M. Pizzotti, F. Tessore and P. Deplano, *Dalton Trans.*, 2012, **41**, 3485–3493.
37 B. Champagne, E. A. Perpète, S. J. A. van Gisbergen, G. J. Snijders, C. Soubra-Ghaoui, K. A. Robins and B. Kirtman, *J. Chem. Phys.*, 1998, **109**, 10489–10495.
38 B. Champagne, E. A. Perpète and D. Jacquemin, *J. Phys. Chem. A*, 2000, **104**, 4755–4763.

39 M. Torrent-Sucarrat, J. M. Anglada and J. M. Luis, *J. Chem. Theory Comput.*, 2011, **7**, 3935–3943.
40 L. E. Johnson, L. R. Dalton and B. H. Robinson, *Acc. Chem. Res.*, 2014, **47**, 3258–3265.
41 M. Guillaume, B. Champagne, N. Markova, V. Enchev and F. Castet, *J. Phys. Chem. A*, 2007, **111**, 9914–9923.
42 F. Mancois, L. Sanguinet, J. L. Pozzo, M. Guillaume, B. Champagne, V. Rodriguez, F. Adamietz, L. Ducasse and F. Castet, *J. Phys. Chem. B*, 2007, **111**, 9795–9802.
43 A. Plaquet, M. Guillaume, B. Champagne, L. Rougier, F. Mancois, V. Rodriguez, J. L. Pozzo, L. Ducasse and F. Castet, *J. Phys. Chem. C*, 2008, **112**, 5638–5645.
44 A. Plaquet, M. Guillaume, B. Champagne, F. Castet, L. Ducasse, J. L. Pozzo and V. Rodriguez, *Phys. Chem. Chem. Phys.*, 2008, **10**, 6223–6232.
45 F. Mancois, J.-L. Pozzo, J. Pan, F. Adamietz, V. Rodriguez, L. Ducasse, F. Castet, A. Plaquet and B. Champagne, *Chem.–Eur. J.*, 2009, **15**, 2560–2571.
46 E. Bogdan, L. Rougier, L. Ducasse, B. Champagne and F. Castet, *J. Phys. Chem. A*, 2010, **114**, 8474–8479.
47 E. Bogdan, A. Plaquet, L. Antonov, V. Rodriguez, L. Ducasse, B. Champagne and F. Castet, *J. Phys. Chem. C*, 2010, **114**, 12760–12768.
48 F. Castet, E. Bogdan, A. Plaquet, L. Ducasse, B. Champagne and V. Rodriguez, *J. Chem. Phys.*, 2012, **136**, 024506.
49 B. Champagne and B. Kirtman, *J. Chem. Phys.*, 2006, **125**, 024101.
50 K. Sasagane, F. Aiga and R. Itoh, *J. Chem. Phys.*, 1993, **99**, 3738–3778.
51 R. E. Stratmann, G. E. Scuseria and M. J. Frisch, *J. Chem. Phys.*, 1998, **109**, 8218–8224.
52 S. Hirata and M. Head-Gordon, *Chem. Phys. Lett.*, 1999, **302**, 375–382.
53 R. Liu, A. Azenkeng, D. Zhou, Y. H. Li, K. D. Glusac and W. F. Sun, *J. Phys. Chem. A*, 2013, **117**, 1907–1917.
54 T. Lu and F. W. Chen, *J. Comput. Chem.*, 2012, **33**, 580–592.
55 P. K. M. Siu, S. W. Lai, W. Lu, N. Zhu and C. A. Che, *Eur. J. Inorg. Chem.*, 2003, 2749–2752.
56 Y. Gao, S. L. Sun, H. L. Xu, L. Zhao and Z. M. Su, *RSC Adv.*, 2014, **4**, 24433–24438.
57 T. Lu and F. W. Chen, *Acta Phys.-Chim. Sin.*, 2012, **28**, 1–18.
58 A. Plaquet, B. Champagne and F. Castet, *Molecules*, 2014, **19**, 10574–10586.
59 K. Sasagane, F. Aiga and R. Itoh, *J. Chem. Phys.*, 1993, **99**, 3738–3778.
60 J. L. Oudar, *J. Chem. Phys.*, 1977, **67**, 446–457.
61 J. L. Oudar and D. S. Chemla, *J. Chem. Phys.*, 1977, **66**, 2664–2668.